

Quantification of long-range transported aeolian dust towards the Indian peninsular region using satellite and ground-based data- a case study during a dust storm over the Arabian Sea

Aswini M. A.¹, Ashwini Kumar^{1*}, Subrata Kumar Das²

¹CSIR-National Institute of Oceanography, Dona Paula, Goa-403004

²Indian Institute of Tropical Meteorology, Dr. HomiBhabha Road, Pashan, Pune – 411 008

* Corresponding author:

Ashwini Kumar

Geological Oceanography Division

CSIR-National Institute of Oceanography

Dona Paula, Goa-403 004

E-mail: ashwinikumarjha@gmail.com, ashwinik@nio.org

Tel: +91 832 2450368, Fax: +91 832 2450602

Abstract

The Arabian Sea is an enclosed basin surrounded by land and is prone to receive large amount of aeolian dust from the continent. This can significantly impact surface water biogeochemical processes. In this study, an attempt has been made to quantify the amount of dust transported from Middle East region to Indian subcontinent (sampling site is Goa; 15.45 °N 73.80 °E; located in the northeast Arabian Sea) via the Arabian Sea. We identified a dust storm episode (02-10 April 2015) in the Arabian Peninsula and its propagation to the study site (Goa) using satellite data (MODIS and CALIPSO). The impact of the dust storm at Goa has been computed using ambient particulate matter concentration and satellite retrieved optical parameter. These observations were further substantiated using ground-based micro-pulse lidar measurement. The daily averaged lidar profile shows relatively high depolarization ratio (0.1-0.25), as well as high daily average backscatter coefficient (up to $0.08 \text{ Sr}^{-1} \text{ Km}^{-1}$) and extinction coefficient (up to 0.9 Km^{-1}) during the storm period compared to non-dusty days. During this period, a two-layer (rich in non-spherical particle) structure with significantly high linear depolarization ratio is observed, indicating the impact of the dust storm at the coastal region of India. Ambient mass concentration of dust estimated using CALIPSO profile are comparable with the gravimetric mass measured from high volume sample collection. The back-trajectory analysis further supports the advection of air-mass from the Middle East to Eastern Arabian Sea. This study highlight the significant role of long-range transport in impacting dust load at the remote/receptor sites.

Keywords: Aerosols; Mineral dust; Arabian Sea; LIDAR; CALIPSO

1. Introduction

Aeolian dust is one of the major components of continental aerosol, which plays a significant role in the various oceanic, atmospheric and terrestrial processes (Arimoto, 2001; Jickells et al., 2005; Mahowald et al., 2017). These dust particles undergo long-range transport under favourable meteorological condition, during which their chemical properties get modified and can significantly impact on regional radiative forcing of receptor regions (Prospero et al., 2002; Arimoto, 2001, Ginoux, 2017;Klingmüller et al., 2019).These dust particles are carrier of several macro- and micro-nutrients from continents and can fertilize marine and terrestrial ecosystems (Duce et al., 2008; Jickells et al., 2005; Rizzolo et al., 2016; Guieu et al., 2019).

The Arabian Sea, located in the Northwestern part of Indian Ocean receives large quantity of dust from surrounding arid/semi-arid region (Tindale and Pease, 1999; Kumar et al., 2008;Lakshmi et al., 2019). Apart from supplying nutrients to Arabian Sea, which significantly modulate primary productivity (Kumar et al., 2008; Banerjee and Kumar, 2014,Shafeeque et al., 2017;Guieu et al., 2019; Bali et al., 2019; Tyagi et al., 2019), these dust particles can also impact on mesoscale processes leading to the break monsoon period during the rainy season over Indian subcontinent (Vinoj et al., 2014; Jin et al., 2016; Dave et al., 2017). In addition, studies have shown that absorbing dust aerosols over the Arabian Sea can enhance the southwest monsoon flow by heating the troposphere (Jin et al., 2015). Due to the seasonality in wind regime, a large variability in the amount as well as type of dust is found over the Arabian Sea(Tindale and Pease, 199;Prospero et al., 2002; Jin et al., 2018; Rashki et al., 2019).During summer months (March-June)episodic wind system such as summer shamal and loo wind are formed over south west Asia (Ramaswamy et al., and reference therein). These episodic wind systems and the continental northerly wind over the Indian peninsular region have potential to carry dust from surrounding Indian sub-continent and Middle-East as well as southwest Asia (Krishna Moorthy et al., 2013, Kumar et al., 2014) towards the Arabian Sea.

Dust storms are frequent phenomenon in the South Asian region during pre-monsoon period (Goudie and Middleton, 2006). Dust storms over Indian subcontinent are mainly derived from the Thar Desert in western part of India, Arabian Peninsula as well as in the desert region spread over Iran and Pakistan (Prospero, 2002; Goudie and Middleton, 2006). A large amount of dust particle gets into the atmosphere due to these storms, which can undergo long-range transport over northern India including Himalayan mountains range (Dey et al., 2004; Hegde et al., 2007; Sharma et al., 2012; Kumar et al., 2014; Kaskaoutis et al., 2015; Kumar et al., 2015; Sarkar et al., 2018) and up to far east region of India (Duchi et al., 2011; Chatterjee et al., 2012). These dust storms are recognized as extreme events which have potential to impact Indian monsoon, hydrological system, regional

radiative forcing and thus on the climate (Gautam et al., 2011; Singh, 2014; Pandey et al., 2017; Patil et al., 2018; Kaskoutis et al., 2018; Sarkar et al., 2018). Considering their importance in regional context of Indian subcontinent, various studies have been undertaken in past to characterize (physical and chemical properties) dust derived from storms and transported over Indian subcontinents (Dey et al., 2004; Gharai et al., 2013; Chinnam et al., 2006; Srivastva et al., 2011; Prasad and Singh, 2007; Sharma et al., 2012; Kumar et al., 2014; Kumar et al., 2015). Most of these studies were focused on the characteristics and impact of dust over the continental site (receptor region). However, there are very few studies which reported on the quantification and their impact over the marine region, particularly over the Arabian Sea (Kumar et al., 2008; Singh et al., 2008). Using satellite observation, Singh et al. (2008) had shown dust induced enhancement in primary productivity (Chlorophyll concentration) during storm events in the Northern Arabian Sea. Another modelling study by Patra et al. (2007) had inferred the role of atmospheric deposition over vertical mixing in amplifying chlorophyll abundance over the Arabian Sea. It is thus crucial to quantify dust supply over the Arabian Sea, during dust storms to understand various biogeochemical processes operating in the surface waters. In this study, we have identified a dust storm in the Middle-East region and tracked dust transport to receptor (sampling) site via the Arabian Sea. Our main objective is the quantification of dust transported to the Arabian Sea and to assess the impact of dust storm at receptor region in Northeast Arabian Sea. This has been done using satellite retrieved data over the source and the Arabian Sea as well as in-situ ground based measurements at the receptor region.

2. Data and Sampling

2.1 Site description

Atmospheric aerosols observations have been carried out in the campus of Council of Scientific and Industrial Research-National Institute of Oceanography (CSIR-NIO), located in Goa (15.45°N, 73.80°E). The measurement site was at a height of about 40 m above mean sea level and ~ 500 m away from the Arabian Sea. The Arabian Sea surrounds this site on its western side and by the Western Ghats on its eastern side (shown in Fig. 1). The site experiences the southwest monsoon (during June to September) and Northeast monsoon (December to February) annually. Aerosol properties are significantly impacted by reversing monsoon wind pattern at this site (Shirodkar and Menon, 2015) wherein, high aerosol optical thickness and large aerosol size particles being observed during summer than winter (Shirodkar and Menon, 2015). In addition, major depressions formed in the North Indian Ocean as well as sea-land breeze plays an important role in modulating the diurnal properties of aerosol over this region (Chazette, 2003).

2.2 Data used

2.2.1 CALIPSO data

In this study, we have used Cloud-Aerosol LIDAR with Orthogonal Polarization (CALIOP) version 4.10 level 2 aerosol layer products to quantify the dust present in the atmospheric column. CALIOP is a two-wavelength, polarization LIDAR (Winker et al., 2007) which is a part of an environmental satellite CALIPSO (Cloud-Aerosol LIDAR and Infrared Pathfinder Satellite Observations). CALIOP measures the vertical profile of atmospheric particles at 532 and 1064 nm near nadir during both day and night. The observations at night time are more accurate compared to that in daytime, because of the interference caused by solar insolation to the total backscatter profile. For this study, we have selected CALIOP night time profiles from 02 -10 April 2015, as the dust storm was started on 02 April ended by 10 April (Fig.1). CALIOP path profile is available with 5 Km horizontal, 60m vertical and 16-days temporal resolution, so we selected large region from 40°–85°E longitude and 5° - 40° N latitude to get adequate number of satellite pass over the study region. Total 13 CALIPSO aerosol path profiles selected out of 65 satellite passes for this study. These selected passes were divided in to three categories near to dust storm generation or source region (S; n = 6), near to the receptor region Goa (G; n = 3) and over the Arabian Sea (C; n = 4) (supplementary Fig. S1 and S2).

Total backscattering coefficient (TBC), depolarization ratio (DR) at 532nm, cloud aerosol-discrimination (CAD)score and extinction quality control (EXT_QC)flag products from the CALIOP measurements were used (https://eosweb.larc.nasa.gov/project/calipso/calipso_table). Aerosol profile data up to 7 Km is selected for the calculation of dust, as dust presence above 7 Km is negligible as compared to the lower altitude. CAD Score (from -20 to -100) is used to filter the aerosol profiles(Liu et al., 2009; Yu et al., 2010). We used EXT_QC flag to remove the false retrieval from TBC values in the level 2 aerosol layers (Winker et al., 2013). Those aerosol layers with values of 0, 1, 16 and 18 were accepted only. The aerosol extinction value retrieved in the Level 2 products are associated with an uncertainty which are discussed in Young et al., (2013).

DR is used to identify the sphericity of particle wherein spherical particles has near zero value, however, non-spherical particle has a typical range from 0.1 to 0.4 (Liu et al., 2008; Murayama et al., 2001). In this study, we used DR threshold values for dust (δd)= 0.20 - 0.30 and for non-dust (δnd) = 0.07 -0.02(Hayasaka et al., 2007, Yu et al., 2015, Yu et al., 2019).The dust backscatter coefficient ($m^{-1} sr^{-1}$) profiles were derived from the profiles of total backscatter and f^d (ratio of dust to total backscatter) following this equation (Yu et al., 2015)

$$f^d = ((\delta - \delta_{nd})(1 + \delta_d)) \div (1 + \delta)(\delta_d + \delta_{nd})$$

Assuming a lidar ratio of 40 Sr at 532 nm, the dust extinction coefficient were calculated (Omar et al., 2010). Subsequently, we calculated the concentration of dust (in g m⁻³) using the mass extinction efficiency (MEE) and dust extinction coefficient. MEE is defined as the ratio of extinction coefficient to aerosol mass concentration taken 0.37 m² g⁻¹ at 532 nm (Kaufman et al., 2005; Maring et al., 2003; Yu et al., 2015).

2.2.2 MODIS data

Moderate Resolution Imaging Spectroradiometers (MODIS) observations have a spatial resolution of 1 km at nadir with a swath width of 2330 km and has 36 spectral bands for the data retrievals (Esaias et al., 1998; Hosoda et al., 2007; Kilpatrick et al., 2015). Level 3 gridded daily mean of Aerosol optical depth (AOD) and angstrom exponent (AE) from MODIS Aqua data product were used in this study (<https://giovanni.gsfc.nasa.gov/giovanni/#>). AOD is available at 550 nm wavelength and AE is available in the spectral bands of 412-470 nm for land. The uncertainty in the AOD data over land is estimated to be $\pm 0.05 \pm 0.20 \times \text{AOD}$ (Levy et al., 2010; Remer et al., 2005, 2008). The Angstrom exponent (AE) provides information on the size of aerosols. The Angstrom exponent is estimated from AOD. It is the negative slope of AOD for a particular wavelength in logarithmic scale. Larger the AE means smaller the particle size. In this study, version 6 products were used which is generated based on the second-generation operational dark target (DT) algorithm (Gupta et al., 2016). The DT algorithm was developed to retrieve aerosols over dark-target surfaces (over oceans) and deep blue algorithms were mainly useful for bright surfaces (over continents). DT can misinterpret the aerosol information above the bright surface like desert.

2.2.3 OMI products

We used aerosol index (AI) data from the Ozone Monitoring Instrument (OMI). The aerosol index is an index that detects the presence of UV-absorbing aerosols such as dust and soot. It is the difference between the observations and model calculations of absorbing and non-absorbing spectral radiance ratios. For the OMI, UV-AI is defined as

$$\text{UV-AI} = 100 \left(\log_{10} \left(\frac{I_{360}}{I_{331}} \right)_{\text{measured}} - \log_{10} \left(\frac{I_{360}}{I_{331}} \right)_{\text{calculated}} \right)$$

(I₃₆₀ / I₃₃₁)_{measured} are the radiances measured at 360 nm and 331 nm and (I₃₆₀ / I₃₃₁)_{calculated} are the calculated radiances at 360 nm and 331 nm assuming a Rayleigh scattering atmosphere. Positive value of UV-AI gives the presence absorbing aerosol such as mineral, volcanic aerosol and biomass burning products. Negative values represent the non-absorbing aerosols like sea

salt. We have used gridded daily mean UV-AI at $1^\circ \times 1^\circ$ spatial resolution (Ahmad et al., 2003) from 01 April to 13 April 2015 at receptor region (15.45°N 73.80°E) from the Giovanni data portal (<https://giovanni.gsfc.nasa.gov/giovanni/#>).

2.2.4 ECMWF-ERA interim data

To study the spatial coverage of wind pattern over the study region, ERA-Interim reanalysis data were used. The ERA-Interim global atmospheric reanalysis product were provided by the European Centre for Medium-Range Weather Forecasts (ECMWF). The gridded u and v components of wind data are available at every 6 hours (http://data-portal.ecmwf.int/data/d/interim_daily/levtype=pl/) at different spatial and temporal resolution as well as pressure and isentropic level. We used u and v wind components at a spatial resolution of $0.75^\circ \times 0.75^\circ$ (Dee et al. 2011). The complete documentation regarding the data is available on the website <http://www.ecmwf.int/publications/newsletters>.

2.2.5 HYSPLIT trajectories model output

Hybrid Single Particle Lagrangian Integrated Trajectory (HYSPLIT) model data are provided by the National Oceanic and Atmospheric Administration (NOAA). The source of air parcel has been calculated with the information of meteorological parameters like rainfall, humidity, temperature and solar radiation flux of different levels from the different regional observations (<https://ready.arl.noaa.gov/HYSPLIT.php>) (Draxler and Rolph, 2003). To identify the source of air parcel, the HYSPLIT backward trajectory model is used. We have computed 7-days back trajectories by running the model at 1200 hours UTC which is 1730 local time for synchronizing our filter based sampling. The back trajectories were computed, ending at our sampling site from 03 April till 13 April at 4 altitude levels (500, 1000, 2000 and 5000 amsl).

2.2.6 Micro Pulse LiDAR data

Vertical profile data were retrieved by operating a micro pulse LIDAR (MPL; model number MPL-4B-IDS-532-AT by Sigma Space Corporation). LIDAR was installed at 40 m height from the mean sea level at our sampling site on July 2013. It detects the backscattered light by atmospheric particulate and calculates its magnitude as a function of time. MPL operates at a wavelength of 532 nm at the rate of 2500 Hz with a pulse width of 9.3 ns and optical laser energy of 6-8 μJ . It has a telescope of 7-8 inches of diameter with focal length of 2.35 m and field of view $81.71 \mu\text{rad}$ which is used for transmitting and receiving the laser signals. The MPL was operated 24 hours a day with 30 m vertical and 30 second temporal resolution. Various parameters viz. depolarization ratio, normalized relative backscatter ($\text{km}^2 \mu\text{s}^{-1} \mu\text{J}^{-1}$), backscatter coefficient ($\text{Km}^{-1} \text{Sr}$) and extinction

coefficient (km^{-1}) were calculated from MPL data set during 01-13 April 2015 (Flynn et al., 2007; Campbell et al., 2003; Fernald 1984).

The magnitude of the backscattered light was used to identify the concentration of particulates and difference between the emitted and received signal was used to calculate the distance to the particulates. Scattering of the particulates measured on the basis of Mie scattering, which determine the size of particulates equal or larger than the size of the emitted the wavelength. Mainly two parameters were used for the study, one is normalized backscatter (NRB) and the other one was depolarization ratio. NRB is calculated using the raw scattered photon counts, laser energy and instrument –specific correction terms and solving the system calibration coefficient through the LIDAR equation (Campbell et al., 2003).

$$NRB(r) = C[\beta_m(r) + \beta_p(r)]T^2(r)$$

Where C is the LIDAR constant, $\beta_m(r)$ is the molecular volume backscattering coefficient and $\beta_p(r)$ particle volume backscattering coefficient, r is the range and $T^2(r)$ is the round-trip total optical transmission.

Depolarization ratio can be defined by following equation:

$$Depolarization\ ratio, Signal = \frac{(NRB\ cross \div NRBco)}{(NRB\ cross \div NRBco + 1)}$$

where NRBCross and NRBCo are the plane of polarization of backscattered laser perpendicular and parallel to emitted laser respectively.

2.3.7 High volume sampling on filters.

We also collected aerosol samples during dust event as well as before and after dust storm (referred as non-dusty samples). A high volume sampler (ENVIROTECH APM 460 DXNL) with PM10 inlet was used to collect aerosol dust. The collected filter samples of PM10 were kept in foil and sealed in zip-lock bags for further gravimetric and chemical analyses. Using the volume of sampled air and weight difference of filter after and before sampling, mass concentration (in $\mu\text{g m}^{-3}$) of PM10 were estimated as

$$Mass\ concentration(\mu\text{gm}^{-3}) = \frac{(finalWt. - InitialWt)}{Vol.\ of\ air\ sampled}$$

3. Results and Discussion

3.1 Identification of dust storm and propagation of dust over the Arabian Sea.

MODIS datasets and truecolour images are widely used for identifying the dust storm over source region as well as its transport to remote locations (Kunte and Aswini, 2015; Singh et al., 2016; Tiwari et al., 2019). Fig. 1 shows the MODIS- Aqua true color images (visible) during the intense dust storm event in the Middle East region. These images depict emission and propagation of dust aerosols between 02 April and 10 April 2015, from Arabian Peninsula towards Indian subcontinent via the Arabian Sea. Dust storms are frequent phenomenon in Middle-East during the pre-monsoon period (Goudie and Middleton, 2006; Prospero et al., 2002, Beegum et al., 2018) and it is one of the major source of dust to the Arabian Sea. A significant amount of dust (26-531 Tg) loading is reported, using airborne, ground-based observations and modeling studies, over the Arabian sea (Huneeus et al., 2011). In our study, a dust storm is identified on 02April (using MODIS image; Fig. 1a) around the southeastern region of the Arabian Peninsula (which includes the Ad-Dhahna desert and Rub- Al-khali desert (Fig. 1a). This storm started propagating towards south eastward direction following the surface wind pattern (shown inFig. 2). Typically, dust storms over the Arabian Peninsula region are mainly caused by pressure gradient existing during the inter-monsoon period. During winter (December-February) months, high-pressure belts lie in North Africa, and northwestern Arabian Peninsula are connected with the Siberian high. This high-pressure buildup starts fading during spring (March-May) months with the simultaneous increase in the surface heating that leads to low pressure in the southeastern side of the Arabian Peninsula which spreads over northern part. This transition in the pressure systems creates an unstable situation and leads to frequent spring dust storms in Saudi Arabia (Al harbi, 2008).

After the generation of this dust storm, it spreads entire southwest Asia, the northern Arabian Sea and Indian region within a week (Fig. 1 c-h). The transport of aeolian dust after the emission is mainly controlled by prevailing wind pattern over the Arabian Sea. During the study period, trade winds and strong westerlies are dominant wind pattern over this region which transports aeolian dust toward south-east Asia and Indian sub-continent (Fig. 2). Surface dust travels towards south following the direction of trade winds (Fig. 2).Upper-level dust transport is carried out by the strong westerlies, wherein dust plume travel towards the Pakistan, Afghanistan, and northern Indian region(Fig. 2 a-b). High speed (more than 10 ms^{-1}) westerlies are dominant over dust source region (Fig. 2b) leading to faster dispersion of dust in a very short time. From 03 April onwards strong winds were observed towards India and blew parallel to the coastal region of the western side of

India as well as toward the southern hemisphere, which brings the dust up to our sampling site (Fig. 2 c).

During our study period, 13 CALIPSO overpasses were retrieved over the study area, as shown in Fig. 2 and more clearly in supplementary Fig. S1. The black and red lines represent the CALIPSO path over and/or near to the source and receptor regions respectively, and the blue line is the path within the Arabian Sea (Fig. 2). CALIPSO products (TBC and DR) give further insight into the distribution of dust aerosols. Using CALIPSO algorithm (Yu et al., 2010; Yu et al., 2015; Yu et al., 2019), we estimated dust concentration (in $\mu\text{g m}^{-3}$), at different altitude and their vertical profile for the available paths at source, Arabian Sea and receptor region which are discussed in section 3.3. This retrieved profile clearly shows the transport of dust from Arabia to Goa via the Arabian Sea and in line with the observation made using MODIS images.

3.2 Impact of dust storm and temporal variability of dust at receptor region (Goa):

Aerosol optical depth (AOD) and angstrom exponent (AE) from MODIS_AQUA deep blue retrieval, and aerosol index (AI) from OMI were used to analyze aerosol load over receptor region during the storm period as well as post-storm days. AOD and AE data calculated by using the blue channel of the satellite instrument, at 550nm wavelength (Hsu et al., 2004, Hsu et al., 2006). AOD is the total integration of extinction by the aerosol present in the entire atmospheric column and AE describes the dependency of the optical thickness on wavelength and it provides an indirect indication of the size of the particles (Dey et al., 2004). The variation of AOD and AE starting from the dust storm day till waning of this event (02 April to 13 April) are shown in Fig. 3. AOD values are low at the beginning and started gradually increasing from 05 April onwards reached maxima on 06 April. Very high AOD value (0.7-0.8) were observed during 06-11 April as compared to non-dusty days, and then sharply decreases to 0.2 on 12 April and onwards. A simultaneous decreasing trend is observed for AE (value goes up to 0) during 06-08 April with a spike observed on 09 April and subsequently shows higher values on the following day. Interestingly, we observed high AE (0.6) and high AOD values on 07 April, which is possibly due to presence of dust mixed with anthropogenic components from local emissions. Vinoj et al. (2008) has observed AE values ranging from 1.4-0.4, for aerosols over the Arabian Sea during winter period, suggesting the impact of anthropogenic sources. These observations indicate the presence of coarse particle in higher concentration mainly because of high dust loading. Similar increase in AOD values (more than 100-200 %) with a corresponding decrease in AE was reported by Dey et al. (2004) over Indo-Gangetic basin. Sharma et al. (2012) have observed the similar signature of optical properties of aerosol during the intense dust storm in Northwestern India during pre-monsoon month of 2010, wherein, they

found high AOD of 1.13 with low AE of 0.31 and AOD of 1.52 with AE of 0.14 at distinct dust storm events

We also investigated the daily variation of the UV aerosol index (AI) for the study period (Fig. 3). The AI is an important parameter which can be used qualitatively, to decouple absorbing (mineral dust, black carbon) and non-absorbing (sulphate) aerosols. A positive value suggests near-UV absorbing aerosols while a negative value indicates non-absorbing aerosols (Prospero et al., 2002). We found a sudden increase in AI, from 0.8 up to 1.6, during the storm period (Fig. 3). This increase further attests to the dominance of the dust particle at the receptor region. Various studies over India have reported a similar increase in AI as well as AOD during the dusty period (Srivastva et al., 2011; Sharma et al., 2012). A study by Tiwari et al. (2016), using space-borne radiometers, have highlighted on the contribution of long-range transported dust aerosols to the Arabian Sea showing very high AI (more than 2).

Along with optical properties, we have measured the total mass concentration of PM₁₀ during the study period and shown in Fig. 3. The mass concentration was very low ($17.4 \mu\text{g m}^{-3}$) on 04 April and increased to more than $100 \mu\text{g m}^{-3}$ and remained above $100 \mu\text{g m}^{-3}$ during the dusty period. These values are higher than the average mass concentration of total suspended particulate ($80.8 \pm 29.5 \mu\text{g m}^{-3}$) reported by Agnihotri et al. (2015). It is important to mention here that we have collected PM₁₀ which gives a lower limit of ambient mass as particles of more than $10 \mu\text{m}$ size were removed during our collection. More than 5 times increase in mass concentration from non-dusty to dusty day supports satellite retrievals indicating the dominance of dust during our study. An increase of more than $150 \mu\text{g m}^{-3}$ from the average PM₁₀ mass is observed over the Indo-Gangetic plane due to the intrusion of aeolian dust during the storm period (Dey et al., 2004). Thus, episodic dust storms, even at a remote location, can significantly impact the aerosol budget at receptor regions.

3.3 Distribution of dust using CALIPSO profile at source, Arabian Sea and receptor region.

The concentrations of dust are significantly different from the surface level to higher altitude with space and time. To understand the vertical distribution of dust, CALIPSO path profiles were used. CALIPSO profiles were investigated at three different regions near to source region (S); near to sampling (receptor) region (G) and over the Arabian Sea (C) (details of CALIPSO profile and their pass are given in section 2.2). Vertically averaged (up to 7 Km) dust concentration for each pass between 02-10 April is shown in Fig. 4. The activation of dust storm near-source region and subsequent uplifting of dust particles are visible in Fig. 4a. A very high dust concentration of more than $1000 \mu\text{g m}^{-3}$, is observed at source region. Latitudinal average ($5-40^{\circ}\text{N}$) dust profile for 02 April

is shown in Fig. 5a, which clearly shows a thick layer of dust ($150\text{-}250 \mu\text{g m}^{-3}$) up to the height of 2 Km. A similar thick layer with reduced dust concentration and with few dust concentration spikes (at 3-5 Km) is observed on 03 April (Fig. 5b). During the transport of dust from the source towards the Arabian Sea, a gradual decrease in dust load is seen in the CALIPSO pass over the Arabian Sea on 05 April (Fig. 4 d). However, the same pass on 05 April, shows the large latitudinal spread of dust with the highest dust concentration around $550 \mu\text{g m}^{-3}$ over the Arabian Sea. We observe minor contribution of dust at different latitudes (Fig. 4c), with spikes of dust above 5 km (Fig. 5c) at receptor region on 04 April. However, these dust are possibly not derived from storm activated in Arabian Peninsula on 02 April rather from other sources. The dust emission was active till 09 April as evident from CALIPSO passes (Fig. 4 c, d, e, f, h), although dust concentration was not as high as observed on 02 April profile. There is large spread in dust layers at later days going up to 5 km on 05 April (Fig. 5d). The height of the layer increased gradually day by day and the maximum extended vertically up to 7 km. Maximum scattering coefficient is (around $0.05 \text{ km}^{-1}\text{Sr}$) observed during the storm days. On 7 April, we find dust concentration above 7 Km height, although less than that of total dust loading. A large spread of dust concentration is observed in the Arabian Sea passes on 05 and 08 April (Fig. 4d and g), clearly highlighting the dispersal of dust through this pathway. Unfortunately, due to the unavailability of CALIPSO passes near the receptor region during the dust event, we could not assess dust loading variation. However, at the end of the dust period, we found the signature of dust loading on 09 April. A bleak signal of dust on 10 April (Fig. 4i and 5 i) CALIPSO pass indicate waning of the dust storm.

3.4 Assessment of dust distribution using MPL vertical profiles at the receptor region

Based on satellite retrieval (AOD, AE and AI) and CALIPSO profile, significant impact of dust storm at our receptor location is identified from 06 April onwards. This is also corroborated by an increase in PM₁₀ mass concentration obtained from high volume samplers. The impact of the dust storm is also evident from the MPL profile shown in Fig. 6, where a gradual increase in the attenuated backscatter signal (NRB; Fig. 6a) and depolarization ratio (DR; Fig. 6b) is observed. The distribution of NRB signal and depolarization ratio from 01 April -13 April 2015 is shown in the height-time cross plot in Fig. 6. The LIDAR profile spanned over 12 days, was categorized into three parts namely (1) Pre-dust event (PrD; 01-04 April) (2) During dust event (DD; 05-09 April) and (3) Post dust event (PoD; 10-13 April), to assess variation in dust abundances. In Fig. 6a, we observe high NRB signal (> 0.3) near the surface and decreases with increase in altitude throughout the study period. However, the corresponding time–altitude variation of DR is significantly different (Fig. 6b), particularly during DD days. A prominent two aerosol layer is observed in the altitude range from

surface to 800 m and 1.6-4 Km showing higher values for DR (0.1-0.4). Such high value is indicative of the dominance of highly non-spherical particles. The layer between two highly loaded layer (with non-spherical particle; 800 m-1.6 km) has very low DR (less than 0.05), suggesting the presence of relatively more spherical particles. MPL study at a station (Trivandrum) located in the Arabian Seacoast of south peninsular India, has observed higher DR (range: 0.1–0.25) between 1 and 3.5 km, during the pre-monsoon period (11-12 June 2008; Mishra et al., 2010) and attributed to the presence of dust. However, DR was very low below 1 Km, during their study period and highlighted on the existence of an elevated dust layer for the first time over the Eastern Arabian Sea. DR values at our study site are relatively higher and stable than those observed at Trivandrum, particularly during storm days. Another similar study by Solanki and Singh (2014), have been carried out on the annual aerosol loading at a remote location in Central Himalaya (Nainital), where they compared the LIDAR with the CALIPSO profile. In their study, they have observed highest loading in spring and summer months (with $3.4 \text{ Mm}^{-1} \text{ Sr}^{-1}$) at 3.3 km. This aerosol layer was found to reach up to 5.6 Km during pre-monsoon season of 2012. In our study, we observed a well-mixed layer in the time–altitude cross-section of NRB and DR, (Fig. 6), subsequent to dust storm (09 April onwards). This mixed layer start to descend to ground level and we observe DR less than 0.1 above 1 Km by 13 April 2015, suggesting the waning of dust storm.

We selected daily average profile from each classified days (i.e. PrD, DD and PoD) and investigated depolarizing ratio, extinction coefficient and backscattering coefficient for each day (Fig. S3). 03 April profile has very low DR (< 0.06) and backscatter values (< 0.05). Dusty day profile on 07 April, show two peaks of high DR (0.17 and 0.22) at a height of ~ 3 Km and just below 1 Km respectively with corresponding high backscattering coefficient ($\geq 0.24 \text{ km}^{-1}$) as well as high extinction coefficient ($> 0.1 \text{ Km}^{-1}$). These observations clearly demonstrate the presence of two-layer of dust at near-surface and at high altitude during the dust event. A similar observation of high backscattering coefficient was reported by Srivastava et al. (2011) at Manora Peak, Nainital, in Central Himalayas, where they attributed such anomalous increase to dust layer derived from the Thar Desert. Veerabhuthiran and Satyanarayana (2003) have observed high extinction coefficient (0.07 Km^{-1}) during the dust period relative to non-dusty days ($0.003\text{-}0.01 \text{ Km}^{-1}$) at Trivandrum, using lidar measurement. Based on this observation, they have highlighted the presence of a dust layer derived from the southwest Asian region at high altitude centered at 4.5 Km.

In order to identify the sources of these particles, we have also examined the air mass back-trajectories at different altitudes in the lower troposphere ending at receptor region using the NOAA ARL HYSPLIT model (https://www.ready.noaa.gov/HYSPLIT_traj.php). Seven days back

trajectories were calculated from 03 to 13 April at 500, 1000, 2000 and 5000m altitude are shown in Fig. 7. The height levels were selected based on the concentration of dust layer observed at the source and receptor region. The back trajectory plot clearly shows that majority of trajectories are passing over Arabian Peninsula and/or nearby coastal region of Arabia as well as over Arabian Sea, during the study period. Lower level trajectories (500-2000m) were observed to pass over the storm region (Rub al Khali, Ad dhahna), Yemen, Gulf of Oman and Persian gulf. We also observed several air parcels coming from the marine region in the Arabian Sea, at an altitude of 1- 2 Km. These trajectories may possibly bring sea-salt along with dust which were dispersed from the storm emission. A study by Pena-Ortiz et al (2013) on global climatological features of sub-tropical jet streams have shown the presence of high speed jet core in the 20-30 °N region. These jet cores have potential to create convection which can uplift ground level dust to higher altitudes which further support for long-range transport of dust. The mechanism of dust upliftment and their propagation due to jet streams resulting in to dust storms, over Saudi Arabia is demonstrated by Alharbi et al (2012). In our study, this high altitude transport is captured in the vertical profile observed at the source and receptor region (Fig. 4; Fig. 5). In addition, we also observed trajectories deriving from continental locations, which can bring air parcels rich in anthropogenic component and can impact the optical properties of dust. Overall, back trajectory analyses support the inferences made from the CALIPSO passes as well as lidar observation over the receptor region.

4. Conclusions

Quantification of dust at the source and receptor region as well as over their transport pathways are important to understand various processes which impact terrestrial and oceanic ecosystem. We report here dust transport over a coastal location in the North East Arabian Sea, resulting from a dust storm activated at Arabian Peninsula, via the Arabian Sea. A suit of proxies (optical parameter derived from satellite retrieval) were used to identify dust storm source and its dispersal towards the Arabian Sea. The dust storm was activated on the 02 April and majority of dust were transported towards southern region, in the Arabian Sea. High aerosol optical depth along with low angstrom exponent (at 550 nm) were observed at the receptor location, indicating the influence of dust at Goa. These observations are corroborated by an increase in aerosol index as well as mass loading (from particulate sampling) during the dusty period compared to non-dusty days. Following the methodology of Yu et al. (2015), we have estimated concentration of dust in vertical profile at the source, receptor and over the Arabian Sea. Typically quantification of dust emission and deposition are done based on the ground level concentration measurements, which may underestimate fluxes as vertical column dust load information is missing. In this context, this study is

possibly first one over the Arabian Sea, which provide concentration estimate of dust up to 7 Km. The impact of dust storm at the receptor location (in the western coast of India) was inferred based on high depolarization ratio and extinction coefficient (obtained from LIDAR) compared to those observed before and after dust event. This study clearly demonstrate the role of long-range transport in impacting regional budget of aeolian dust at far remote locations. This type of studies are necessary to reduce uncertainty associated estimation of dust on global scale which has implication to oceanic biogeochemical processes.

Acknowledgment:

Funding for this research is supported by CSIR Networked Project GEOSINK. Ashwini Kumar was funded by the Department of Science and Technology, Govt. of India under the INSPIRE Faculty scheme (IFA13-EAS-13). Aswini, M. A. was funded by CSIR Senior research fellowship (31/26(0325)/2019-EMR-I). We gratefully acknowledge the NOAA Air Resources Laboratory (ARL) for the provision of the HYSPLIT transport and dispersion model (<http://www.ready.noaa.gov>) used in this publication. We thank the two anonymous reviewers and editor for their valuable comments/suggestions, which helped in improving this paper.

References

- Agnihotri, R., Karapurkar, S.G., Sarma, V.V.S.S., Yadav, K., Kumar, M.D., Sharma, C., Prasad, M.V.S.N., 2015. Stable isotopic and chemical characteristics of bulk aerosols during winter and summer season at a station in Western Coast of India (Goa). *Aerosol Air Qual. Res.* 15, 888–900. <https://doi.org/10.4209/aaqr.2014.07.0127>
- Ahmad, S.P., Levelt, P.F., Bhartia, P.K., Hilsenrath, E., Leppelmeier, G.W., Johnson, J.E., 2003. Atmospheric products from the ozone monitoring instrument (OMI). *Earth Obs. Syst.* VIII 5151, 619. <https://doi.org/10.1117/12.506042>
- Alharbi, B.H., Maghrabi, A., Tapper, N., 2013. The March 2009 Dust Event in Saudi Arabia: Precursor and Supportive Environment. *Bull. Am. Meteorol. Soc.* 94, 515–528. <https://doi.org/10.1175/BAMS-D-11-00118.1>
- Alharbi, B.H.A., 2009. Airborne dust in Saudi Arabia : source areas, entrainment, simulation and composition. <https://doi.org/10.4225/03/58802953881A8>
- Arimoto, R., 2001. Eolian dust and climate: Relationship to sources, tropospheric chemistry, transport and deposition. *Earth-Science Rev.* 54, 29–42. [https://doi.org/10.1016/S0012-8252\(01\)00040-X](https://doi.org/10.1016/S0012-8252(01)00040-X)
- Bali, K., Mishra, A.K., Singh, S., Chandra, S., Lehahn, Y., 2019. Impact of dust storm on phytoplankton bloom over the Arabian Sea: a case study during March 2012. *Environ. Sci. Pollut. Res.* 26, 11940–11950. <https://doi.org/10.1007/s11356-019-04602-7>
- Beegum, S.N., Gherboudj, I., Chaouch, N., Temimi, M., Ghedira, H., 2018. Simulation and analysis of synoptic scale dust storms over the Arabian Peninsula. *Atmos. Res.* 199, 62–81. <https://doi.org/10.1016/j.atmosres.2017.09.003>
- Banerjee, P., Prasanna Kumar, S., 2014. Dust-induced episodic phytoplankton blooms in the Arabian Sea during winter monsoon. *J. Geophys. Res. Ocean.* 119, 7123–7138. <https://doi.org/10.1002/2014JC010304>
- Campbell, J.R., Welton, E.J., Spinhirne, J.D., Ji, Q., Tsay, S.C., Piketh, S.J., Barenbrug, M., Holben, B.N., 2003. Micropulse lidar observations of tropospheric aerosols over northeastern South Africa during the ARREX and SAFARI 2000 dry season experiments. *J. Geophys. Res. D Atmos.* 108, 1–19. <https://doi.org/10.1029/2002jd002563>
- Chatterjee, A., Ghosh, S.K., Adak, A., Singh, A.K., Devara, P.C.S., Raha, S., 2012. Effect of Dust and Anthropogenic Aerosols on Columnar Aerosol Optical Properties over Darjeeling (2200 m asl), Eastern Himalayas , India 7. <https://doi.org/10.1371/journal.pone.0040286>
- Chazette, P., 2003. The monsoon aerosol extinction properties at Goa during INDOEX as measured with lidar. *J. Geophys. Res. D Atmos.* 108, 1–12. <https://doi.org/10.1029/2002jd002074>
- Chinnam, N., Dey, S., Tripathi, S.N., Sharma, M., 2006. Dust events in Kanpur, northern India: Chemical evidence for source and implications to radiative forcing. *Geophys. Res. Lett.* 33, 1–4. <https://doi.org/10.1029/2005GL025278>

- Dave, P., Bhushan, M., Venkataraman, C., 2017. Aerosols cause intraseasonal short-term suppression of Indian monsoon rainfall. *Sci. Rep.* 7, 17347. <https://doi.org/10.1038/s41598-017-17599-1>
- Dee, D.P., Uppala, S.M., Simmons, A.J., Berrisford, P., Poli, P., Kobayashi, S., Andrae, U., Balmaseda, M.A., Balsamo, G., Bauer, P., Bechtold, P., Beljaars, A.C.M., van de Berg, L., Bidlot, J., Bormann, N., Delsol, C., Dragani, R., Fuentes, M., Geer, A.J., Haimberger, L., Healy, S.B., Hersbach, H., Hólm, E. V., Isaksen, I., Kållberg, P., Köhler, M., Matricardi, M., McNally, A.P., Monge-Sanz, B.M., Morcrette, J.J., Park, B.K., Peubey, C., de Rosnay, P., Tavolato, C., Thépaut, J.N., Vitart, F., 2011. The ERA-Interim reanalysis: Configuration and performance of the data assimilation system. *Q. J. R. Meteorol. Soc.* 137, 553–597. <https://doi.org/10.1002/qj.828>
- Dey, S., Tripathi, S.N., Singh, R.P., Holben, B.N., 2004. Influence of dust storms on the aerosol optical properties over the Indo-Gangetic basin. *J. Geophys. Res. D Atmos.* 109, 1–13. <https://doi.org/10.1029/2004JD004924>
- Draxler, R. R. and Rolph, G. D.: HYSPLIT (Hybrid Single-Particle Lagrangian Integrated Trajectory) Model access via NOAA ARL READY Website (<http://www.arl.noaa.gov/HYSPLIT.php>). NOAA Air Resources Laboratory, Silver Spring, MD, 2003.
- Duce, R.A., LaRoche, J., Altieri, K., Arrigo, K.R., Baker, A.R., Capone, D.G., Cornell, S., Dentener, F., Galloway, J., Ganeshram, R.S., Geider, R.J., Jickells, T., Kuypers, M.M., Langlois, R., Liss, P.S., Liu, S.M., Middelburg, J.J., Moore, C.M., Nickovic, S., Oschlies, A., Pedersen, T., Prospero, J., Schlitzer, R., Seitzinger, S., Sorensen, L.L., Uematsu, M., Ulloa, O., Voss, M., Ward, B., Zamora, L., 2008. Impacts of atmospheric anthropogenic nitrogen on the open ocean. *Science* (80-). 320, 893–897. <https://doi.org/10.1126/science.1150369>
- Duchi, R., Cristofanelli, P., Marinoni, A., Laj, P., Marcq, S., Villani, P., Sellegri, K., Angelini, F., Calzolari, F., Gobbi, G.P., Verza, G.P., Vuillermoz, E., Sapkota, A., Bonasoni, P., 2011. Continuous observations of synoptic-scale dust transport at the Nepal Climate Observatory-Pyramid (5079\,m\,a.s.l.) in the Himalayas. *Atmos. Chem. Phys. Discuss.* 11, 4229–4261. <https://doi.org/10.5194/acpd-11-4229-2011>
- Esaias, W.E., Abbott, M.R., Barton, I., Brown, O.B., Campbell, J.W., Carder, K.L., Clark, D.K., Evans, R.H., Hoge, F.E., Gordon, H.R., Balch, W.M., Letelier, R., Minnett, P.J., 1998. An Overview of MODIS Capabilities for Ocean Science Observations 36, 1250–1265.
- Fernald, F.G., 1984. Analysis of atmospheric lidar observations : some comments © 1984 Optical Society of America .
- Flynn, C.J., Mendoza, A., Zheng, Y., Mathur, S., 2007. Novel polarization-sensitive micropulse lidar measurement technique. *Opt. Express* 15, 2785. <https://doi.org/10.1364/oe.15.002785>
- Gautam, R., Hsu, N.C., Tsay, S.C., Lau, K.M., Holben, B., Bell, S., Smirnov, A., Li, C., Hansell, R., 2011. and Physics Accumulation of aerosols over the Indo-Gangetic plains and southern slopes of the Himalayas : distribution , properties and radiative effects during the 2009 pre-monsoon season 12841–12863. <https://doi.org/10.5194/acp-11-12841-2011>

- Gharai, B., Jose, S., Mahalakshmi, D. V., 2013. Monitoring intense dust storms over the Indian region using satellite data - a case study. *Int. J. Remote Sens.* 34, 7038–7048. <https://doi.org/10.1080/01431161.2013.813655>
- Ginoux, P., 2017. Atmospheric chemistry: Warming or cooling dust? *Nat. Geosci.* 10, 246–247. <https://doi.org/10.1038/ngeo2923>
- Guieu, C., Al Azhar, M., Aumont, O., Mahowald, N., Levy, M., Ethé, C., Lachkar, Z., 2019. Major Impact of Dust Deposition on the Productivity of the Arabian Sea. *Geophys. Res. Lett.* 6736–6744. <https://doi.org/10.1029/2019GL082770>
- Goudie, A. S., Middleton, N. J., 2006: *Desert Dust in the Global System*. Springer, 287.
- Gupta, P., Levy, R.C., Mattoo, S., Remer, L.A., Munchak, L.A., 2016. A surface reflectance scheme for retrieving aerosol optical depth over urban surfaces in MODIS Dark Target retrieval algorithm 3293–3308. <https://doi.org/10.5194/amt-9-3293-2016>
- Hayasaka, T., Satake, S., Shimizu, A., Sugimoto, N., Matsui, I., Aoki, K., Muraji, Y., 2007. Vertical distribution and optical properties of aerosols observed over Japan during the Atmospheric Brown Clouds-East Asia Regional Experiment 2005. *J. Geophys. Res. Atmos.* 112. <https://doi.org/10.1029/2006JD008086>
- Hegde, P., Pant, P., Naja, M., Dumka, U.C., Sagar, R., 2007. South Asian dust episode in June 2006: Aerosol observations in the central Himalayas. *Geophys. Res. Lett.* 34, 1–5. <https://doi.org/10.1029/2007GL030692>
- Hosoda, K., Murakami, H., Sakaida, F., Kawamura, H., 2007. Algorithm and validation of sea surface temperature observation using MODIS sensors aboard terra and aqua in the western North Pacific. *J. Oceanogr.* 63, 267–280. <https://doi.org/10.1007/s10872-007-0027-4>
- Hsu, N.C., Tsay, S.C., King, M.D., Herman, J.R., 2006. Deep Blue retrievals of Asian aerosol properties during ACE-Asia. *IEEE Trans. Geosci. Remote Sens.* 44, 3180–3195. <https://doi.org/10.1109/TGRS.2006.879540>
- Hsu, N.C., Tsay, S.C., King, M.D., Herman, J.R., 2004. Aerosol properties over bright-reflecting source regions. *IEEE Trans. Geosci. Remote Sens.* 42, 557–569. <https://doi.org/10.1109/TGRS.2004.824067>
- Huneeus, N., Schulz, M., Balkanski, Y., Griesfeller, J., Prospero, J., Kinne, S., Bauer, S., Boucher, O., Chin, M., Dentener, F., Diehl, T., Easter, R., Fillmore, D., Ghan, S., Ginoux, P., Grini, A., Horowitz, L., Koch, D., Krol, M.C., Landing, W., Liu, X., Mahowald, N., Miller, R., Morcrette, J.J., Myhre, G., Penner, J., Perlwitz, J., Stier, P., Takemura, T., Zender, C.S., 2011. Global dust model intercomparison in AeroCom phase i. *Atmos. Chem. Phys.* 11, 7781–7816. <https://doi.org/10.5194/acp-11-7781-2011>
- Jickells, T.D., An, Z.S., Andersen, K.K., Baker, A.R., Bergametti, C., Brooks, N., Cao, J.J., Boyd, P.W., Duce, R.A., Hunter, K.A., Kawahata, H., Kubilay, N., LaRoche, J., Liss, P.S., Mahowald, N., Prospero, J.M., Ridgwell, A.J., Tegen, I., Torres, R., 2005. Global iron connections between desert dust, ocean biogeochemistry, and climate. *Science* (80-.). 308, 67–71. <https://doi.org/10.1126/science.1105959>

- Jin, Q., Wei, J., Pu, B., Yang, Z.L., Parajuli, S.P., 2018. High Summertime Aerosol Loadings Over the Arabian Sea and Their Transport Pathways. *J. Geophys. Res. Atmos.* 123, 10,568-10,590. <https://doi.org/10.1029/2018JD028588>
- Jin, Q., Wei, J., Yang, Z.L., Pu, B., Huang, J., 2015. Consistent response of Indian summer monsoon to Middle East dust in observations and simulations. *Atmos. Chem. Phys. Discuss.* 15, 15571–15619. <https://doi.org/10.5194/acpd-15-15571-2015>
- Jin, Q., Yang, Z.L., Wei, J., 2016. Seasonal responses of Indian summer monsoon to dust aerosols in the middle East, India, and China. *J. Clim.* 29, 6329–6349. <https://doi.org/10.1175/JCLI-D-15-0622.1>
- Kaskaoutis, D.G., Rashki, A., Houssos, E.E., Mofidi, A., Goto, D., Bartzokas, A., Francois, P., Legrand, M., 2015. Meteorological aspects associated with dust storms in the Sistan region , southeastern Iran. *Clim. Dyn.* 407–424. <https://doi.org/10.1007/s00382-014-2208-3>
- Kaskaoutis, D.G., Houssos, E.E., Solmon, F., Legrand, M., Rashki, A., Dumka, U.C., Francois, P., Gautam, R., Singh, R.P., 2018. Impact of atmospheric circulation types on southwest Asian dust and Indian summer monsoon rainfall. *Atmos. Res.* 201, 189–205. <https://doi.org/https://doi.org/10.1016/j.atmosres.2017.11.002>
- Kaufman, Y.J., Koren, I., Remer, L.A., Tanré, D., Ginoux, P., Fan, S., 2005. Dust transport and deposition observed from the Terra-Moderate Resolution Imaging Spectroradiometer (MODIS) spacecraft over the Atlantic Ocean. *J. Geophys. Res. D Atmos.* 110, 1–16. <https://doi.org/10.1029/2003JD004436>
- Kilpatrick, K.A., Podestá, G., Walsh, S., Williams, E., Halliwell, V., Szczodrak, M., Brown, O.B., Minnett, P.J., Evans, R., 2015. Remote Sensing of Environment A decade of sea surface temperature from MODIS. *Remote Sens. Environ.* 165, 27–41. <https://doi.org/10.1016/j.rse.2015.04.023>
- Klingmüller, K., Lelieveld, J., Karydis, V.A., Stenchikov, G.L., 2019. Direct radiative effect of dust-pollution interactions. *Atmos. Chem. Phys.* 19, 7397–7408. <https://doi.org/10.5194/acp-19-7397-2019>
- Krishna Moorthy, K., Suresh Babu, S., Manoj, M.R., Satheesh, S.K., 2013. Buildup of aerosols over the Indian Region. *Geophys. Res. Lett.* 40, 1011–1014. <https://doi.org/10.1002/grl.50165>
- Kumar, A., Sudheer, A.K., Sarin, M.M., 2008. Chemical characteristics of aerosols in MABL of bay of Bengal and Arabian sea during spring inter-monsoon: A comparative study. *J. Earth Syst. Sci.* 117, 325–332. <https://doi.org/10.1007/s12040-008-0035-9>
- Kumar, R., Barth, M.C., Madronich, S., Naja, M., Carmichael, G.R., Pfister, G.G., Knote, C., Brasseur, G.P., 2014. Effects of dust aerosols on tropospheric chemistry during a typical pre-monsoon season dust storm in northern India 6813–6834. <https://doi.org/10.5194/acp-14-6813-2014>
- Kumar, Sarvan, Kumar, Sanjay, Kaskaoutis, D.G., Singh, R.P., Singh, R.K., Mishra, A.K., Srivastava, M.K., Singh, A.K., 2015. Meteorological , atmospheric and climatic perturbations during major dust storms over Indo-Gangetic Basin. *AEOLIAN Res.* 17, 15–31. <https://doi.org/10.1016/j.aeolia.2015.01.006>

- Kunte, P.D., M.A., A., 2015. Detection and monitoring of super sandstorm and its impacts on Arabian Sea-Remote sensing approach. *Atmos. Res.* 160, 109–125. <https://doi.org/10.1016/j.atmosres.2015.03.003>
- Lakshmi, N.B., Babu, S.S., Nair, V.S., 2019. Recent Regime Shifts in Mineral Dust Trends over South Asia from Long-Term CALIPSO Observations. *IEEE Trans. Geosci. Remote Sens.* 57, 4485–4489. <https://doi.org/10.1109/TGRS.2019.2891338>
- Levy, R.C., Remer, L., County, B., 2010. and Physics Global evaluation of the Collection 5 MODIS dark-target aerosol products over land. <https://doi.org/10.5194/acp-10-10399-2010>
- Li, Z., Zhao, X., Kahn, R., Mishchenko, M., Remer, L., Lee, K., Wang, M., Laszlo, I., Nakajima, T., 2009. *Annales Geophysicae* Uncertainties in satellite remote sensing of aerosols and impact on monitoring its long-term trend : a review and perspective 2755–2770.
- Liu, Z., Liu, D., Huang, J., Vaughan, M., Uno, I., Sugimoto, N., Kittaka, C., Trepte, C., Wang, Z., Hostetler, C., Winker, D., 2008. Airborne dust distributions over the Tibetan Plateau and surrounding areas derived from the first year of CALIPSO lidar observations. *Atmos. Chem. Phys.* 8, 5045–5060. <https://doi.org/10.5194/acp-8-5045-2008>
- Liu, Z., Vaughan, M., Winker, D., Kittaka, C., Getzewich, B., Kuehn, R., Omar, A., Powell, K., Trepte, C., Hostetler, C., 2009. The CALIPSO lidar cloud and aerosol discrimination: Version 2 algorithm and initial assessment of performance. *J. Atmos. Ocean. Technol.* 26, 1198–1213. <https://doi.org/10.1175/2009JTECHA1229.1>
- Mahowald, N.M., Scanza, R., Brahney, J., Goodale, C.L., Hess, P.G., Moore, J.K., Neff, J., 2017. Aerosol Deposition Impacts on Land and Ocean Carbon Cycles. *Curr. Clim. Chang. Reports* 3, 16–31. <https://doi.org/10.1007/s40641-017-0056-z>
- Maring, H., Savoie, D.L., Izaguirre, M.A., Custals, L., Reid, J.S., 2003. Mineral dust aerosol size distribution change during atmospheric transport. *J. Geophys. Res. D Atmos.* 108, 1–6. <https://doi.org/10.1029/2002jd002536>
- Mishra, M.K., Rajeev, K., Thampi, B. V., Parameswaran, K., Nair, A.K.M., 2010. Micro pulse lidar observations of mineral dust layer in the lower troposphere over the southwest coast of Peninsular India during the Asian summer monsoon season. *J. Atmos. Solar-Terrestrial Phys.* 72, 1251–1259. <https://doi.org/10.1016/j.jastp.2010.08.012>
- Murayama, T., Sugimoto, N., Uno, I., Kinoshita, K., Aoki, K., Hagiwara, N., Liu, Z., Matsui, I., Sakai, T., Shibata, T., Arao, K., Sohn, B.J., Won, J.G., Yoon, S.C., Li, T., Zhou, J., Hu, H., Abo, M., Iokibe, K., Koga, R., Iwasaka, Y., 2001. Ground-based network observation of Asian dust events of April 1998 in east Asia. *J. Geophys. Res. Atmos.* 106, 18345–18359. <https://doi.org/10.1029/2000JD900554>
- Omar, A., Liu, Z., Vaughan, M., Thornhill, K., Kittaka, C., Ismail, S., Hu, Y., Chen, G., Powell, K., Winker, D., Trepte, C., Winstead, E., Anderson, B., 2010. Extinction-to-backscatter ratios of Saharan dust layers derived from in situ measurements and CALIPSO overflights during NAMMA. *J. Geophys. Res. Atmos.* 115, 1–21. <https://doi.org/10.1029/2010JD014223>

- Pandey, S.K., Vinoj, V., Landu, K., Babu, S.S., 2017. Declining pre-monsoon dust loading over South Asia: Signature of a changing regional climate. *Sci. Rep.* 1–10. <https://doi.org/10.1038/s41598-017-16338-w>
- Patil, N., Venkataraman, C., Muduchuru, K., Ghosh, S., Mondal, A., 2019. Disentangling sea-surface temperature and anthropogenic aerosol influences on recent trends in South Asian monsoon rainfall. *Clim. Dyn.* 52, 2287–2302. <https://doi.org/10.1007/s00382-018-4251-y>
- Patra, P.K., Kumar, M.D., Mahowald, N., Sarma, V.V.S.S., 2007. Atmospheric deposition and surface stratification as controls of contrasting chlorophyll abundance in the North Indian Ocean. *J. Geophys. Res. Ocean.* 112, 1–14. <https://doi.org/10.1029/2006JC003885>
- Pena-ortiz, C., Gallego, D., Ribera, P., Ordonez, P., Alvarez-castro, M.D.C., 2013. Observed trends in the global jet stream characteristics during the second half of the 20th century 118, 2702–2713.
- Prasad, A.K., Singh, R.P., 2007. Comparison of MISR-MODIS aerosol optical depth over the Indo-Gangetic basin during the winter and summer seasons (2000-2005). *Remote Sens. Environ.* 107, 109–119. <https://doi.org/10.1016/j.rse.2006.09.026>
- Prospero, J.M., Ginoux, P., Torres, O., Nicholson, S.E., Gill, T.E., 2002. Environmental characterization of global sources of atmospheric soil dust identified with the Nimbus 7 Total Ozone Mapping Spectrometer (TOMS) absorbing aerosol product. *Rev. Geophys.* 40, 1–31. <https://doi.org/10.1029/2000RG000095>
- Ramaswamy, V., Muraleedharan, P.M., Babu, C.P., 2017. Mid-troposphere transport of Middle-East dust over the Arabian Sea and its effect on rainwater composition and sensitive ecosystems over India. *Sci. Rep.* 7, 1–8. <https://doi.org/10.1038/s41598-017-13652-1>
- Rashki, A., Kaskaoutis, D.G., Mofidi, A., Minvielle, F., Chiapello, I., Legrand, M., Dumka, U.C., Francois, P., 2019. Effects of Monsoon, Shamal and Levar winds on dust accumulation over the Arabian Sea during summer – The July 2016 case. *Aeolian Res.* 36, 27–44. <https://doi.org/10.1016/j.aeolia.2018.11.002>
- Remer, L.A., Kleidman, R.G., Levy, R.C., Kaufman, Y.J., Mattoo, S., Martins, J.V., Ichoku, C., Koren, I., Yu, H., Holben, B.N., 2008. Global aerosol climatology from the MODIS satellite sensors 113, 1–18. <https://doi.org/10.1029/2007JD009661>
- Rizzolo, J.A., Barbosa, C.G.G., Borillo, G.C., Godoi, A.F.L., Souza, R.A.F., Andreoli, R. V., Manzi, A.O., Sá, M.O., Alves, E.G., Pöhlker, C., Angelis, I.H., Ditas, F., Saturno, J., Moran-Zuloaga, D., Rizzo, L. V., Rosário, N.E., Pauliquevis, T., Yamamoto, C.I., Andreae, M.O., Taylor, P.E., Godoi, R.H.M., 2016. Mineral nutrients in Saharan dust and their potential impact on Amazon rainforest ecology. *Atmos. Chem. Phys. Discuss.* 1–43. <https://doi.org/10.5194/acp-2016-557>
- Sarkar, S., 2019. Impact of Deadly Dust Storms (May 2018) on Air Quality , Meteorological , and Atmospheric Parameters Over the Northern Parts of India. *GeoHealth* 67–80. <https://doi.org/10.1029/2018GH000170>
- Shafeeque, M., Sathyendranath, S., George, G., Balchand, A.N., Platt, T., 2017. Comparison of seasonal cycles of phytoplankton chlorophyll, aerosols, winds and sea-surface temperature off somalia. *Front. Mar. Sci.* 4, 1–15. <https://doi.org/10.3389/fmars.2017.00386>

- Sharma, D., Singh, D., Kaskaoutis, D.G., 2012. Impact of two intense dust storms on aerosol characteristics and radiative forcing over Patiala, Northwestern India. *Adv. Meteorol.* 2012. <https://doi.org/10.1155/2012/956814>
- Shirodkar, S., Menon, H.B., 2015. Aerosol optical properties over a coastal site in Goa, along the west coast of India. *J. Atmos. Solar-Terrestrial Phys.* 130–131, 182–189. <https://doi.org/10.1016/j.jastp.2015.06.002>
- Singh, A., Tiwari, Shani, Sharma, D., Singh, D., Tiwari, Suresh, Srivastava, A.K., Rastogi, N., Singh, A.K., 2016. Characterization and radiative impact of dust aerosols over northwestern part of India: a case study during a severe dust storm. *Meteorol. Atmos. Phys.* 128, 779–792. <https://doi.org/10.1007/s00703-016-0445-1>
- Singh, R. P., 2014. Dust storms and their influence on atmospheric parameters over the Indo-Gangetic plains. *Geospatial technologies and climate change.* 21–35. Cham: Springer. https://doi.org/10.1007/978-3-319-01689-4_2
- Singh, R.P., Prasad, A.K., Kayetha, V.K., Kafatos, M., 2008. Enhancement of oceanic parameters associated with dust storms using satellite data. *J. Geophys. Res. Ocean.* 113, 1–13. <https://doi.org/10.1029/2008JC004815>
- Solanki, R., Singh, N., 2014. LiDAR observations of the vertical distribution of aerosols in free troposphere: Comparison with CALIPSO level-2 data over the central Himalayas. *Atmos. Environ.* 99, 227–238. <https://doi.org/10.1016/j.atmosenv.2014.09.083>
- Srivastava, A.K., Pant, P., Hegde, P., Singh, S., Dumka, U.C., Naja, M., Singh, N., Bhavanikumar, Y., 2011. The influence of a south asian dust storm on aerosol radiative forcing at a high-altitude station in central Himalayas. *Int. J. Remote Sens.* 32, 7827–7845. <https://doi.org/10.1080/01431161.2010.531781>
- Tindale, N.W., Pease, P.P., 1999. Aerosols over the Arabian Sea: Atmospheric transport pathways and concentrations of dust and sea salt. *Deep. Res. Part II Top. Stud. Oceanogr.* 46, 1577–1595. [https://doi.org/10.1016/S0967-0645\(99\)00036-3](https://doi.org/10.1016/S0967-0645(99)00036-3)
- Tiwari, S., Kumar, A., Pratap, V., Singh, A.K., 2019. Assessment of two intense dust storm characteristics over Indo – Gangetic basin and their radiative impacts: A case study. *Atmos. Res.* 228, 23–40. <https://doi.org/10.1016/j.atmosres.2019.05.011>
- Tiwari, S., Mishra, A.K., Singh, A.K., 2016. Aerosol climatology over the Bay of Bengal and Arabian Sea inferred from space-borne radiometers and lidar observations. *Aerosol Air Qual. Res.* 16, 2855–2868. <https://doi.org/10.4209/aaqr.2015.06.0406>
- Tyagi, G., Babu, K.N., Solanki, H.A., 2019. Monitoring bio-optical response of coastal waters surrounding the Indian subcontinent to atmospheric dust deposition using satellite data. *Environ. Sci. Pollut. Res.* <https://doi.org/10.1007/s11356-019-07134-2>
- Veerabuthiran, S., Satyanarayana, M., 2003. Lidar observations on atmospheric dust transported from south-west Asia to Indian west coast region: A case study of colour rain event occurred during July 2001. *Indian J. Radio Sp. Phys.* 32, 158–165.

- Vinoj, V., Rasch, P.J., Wang, H., Yoon, J.H., Ma, P.L., Landu, K., Singh, B., 2014. Short-term modulation of Indian summer monsoon rainfall by West Asian dust. *Nat. Geosci.* 7, 308–313. <https://doi.org/10.1038/ngeo2107>
- Vinoj, V., Satheesh, S.K., Moorthy, K.K., 2008. Aerosol characteristics at a remote island : Minicoy in southern Arabian Sea 389–397.
- Winker, D.M., Tackett, J.L., Getzewich, B.J., Liu, Z., Vaughan, M.A., Rogers, R.R., 2013. The global 3-D distribution of tropospheric aerosols as characterized by CALIOP. *Atmos. Chem. Phys.* 13, 3345–3361. <https://doi.org/10.5194/acp-13-3345-2013>
- Winker, D.M., Hunt, W.H., McGill, M.J., 2007. Initial performance assessment of CALIOP. *Geophys. Res. Lett.* 34, 1–5. <https://doi.org/10.1029/2007GL030135>.
- Young, S. A., Vaughan, M. A., Kuehn, R. E., Winker, D.M., 2013. The Retrieval of Profiles of Particulate Extinction from Cloud-Aerosol Lidar Infrared Pathfinder Satellite Observations(CALIPSO) Data: Uncertainty and Error Sensitivity Analyses, *J. Atmos. Oceanic Technol.*, doi:10.1175/JTECH-D-12-00046.
- Yu, H., Tan, Q., Chin, M., Remer, L.A., Kahn, R.A., Bian, H., Kim, D., Zhang, Z., Yuan, T., Omar, A.H., Winker, D.M., Levy, R.C., Kalashnikova, O., Crepeau, L., Capelle, V., Chédin, A., 2019. Estimates of African Dust Deposition Along the Trans-Atlantic Transit Using the Decadelong Record of Aerosol Measurements from CALIOP, MODIS, MISR, and IASI. *J. Geophys. Res. Atmos.* 124, 7975–7996. <https://doi.org/10.1029/2019JD030574>
- Yu, H., Chin, M., Bian, H., Yuan, T., Prospero, J.M., Omar, A.H., Remer, L.A., Winker, D.M., Yang, Y., Zhang, Y., Zhang, Z., 2015. Quantification of trans-Atlantic dust transport from seven-year (2007-2013) record of CALIPSO lidar measurements. *Remote Sens. Environ.* 159, 232–249. <https://doi.org/10.1016/j.rse.2014.12.010>
- Yu, H., Chin, M., Winker, D.M., Omar, A.H., Liu, Z., Kittaka, C., Diehl, T., 2010. Global view of aerosol vertical distributions from CALIPSO lidar measurements and GOCART simulations: Regional and seasonal variations. *J. Geophys. Res. Atmos.* 115, 1–19. <https://doi.org/10.1029/2009JD013364>

Figures:

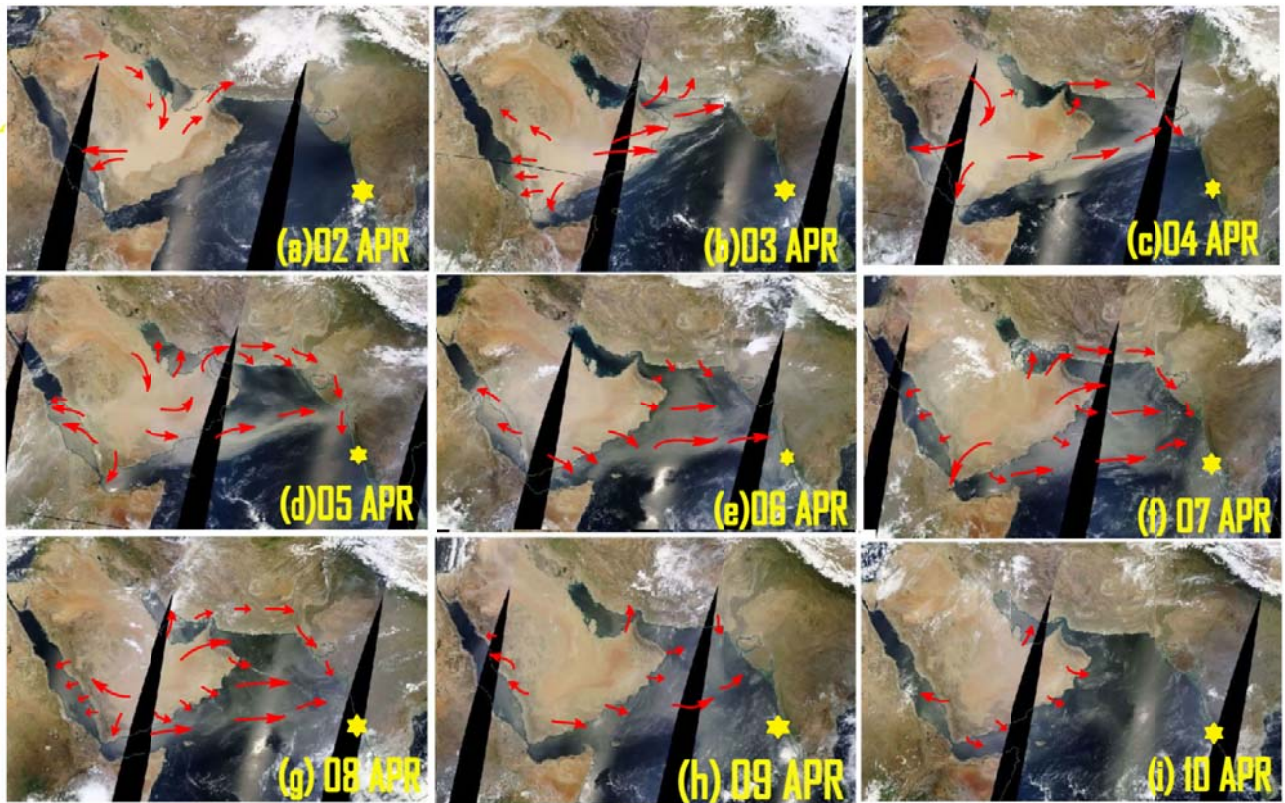


Fig. 1: True color image of MODIS Aqua satellite from 02 April - 10 April 2015 during the dust storm event. Red arrows show dispersal and transport of dust downwind to Arabian Sea and Goa (marked as yellow filled star). Images are generated from earth observing system data and information system link (<https://worldview.earthdata.nasa.gov>).

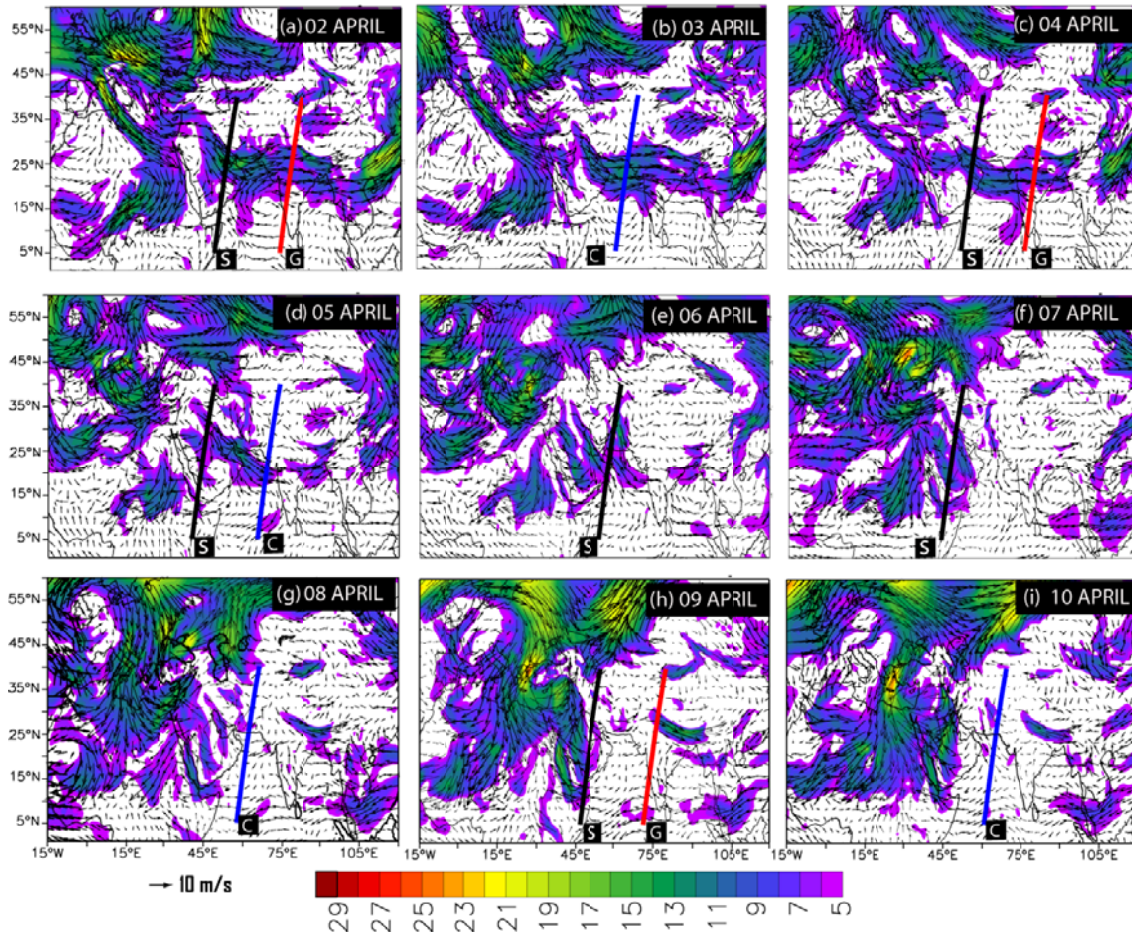


Fig. 2: Daily mean wind speed (shaded) $> 5\text{m/s}$ and wind components (vector) at 850 hpa pressure level plotted over a study region from 02 April to 10 April 2015. Solid bold lines represent the CALIPSO profile path retrieved at various locations in the study region (see supplementary Fig. S1 and text for detail description)

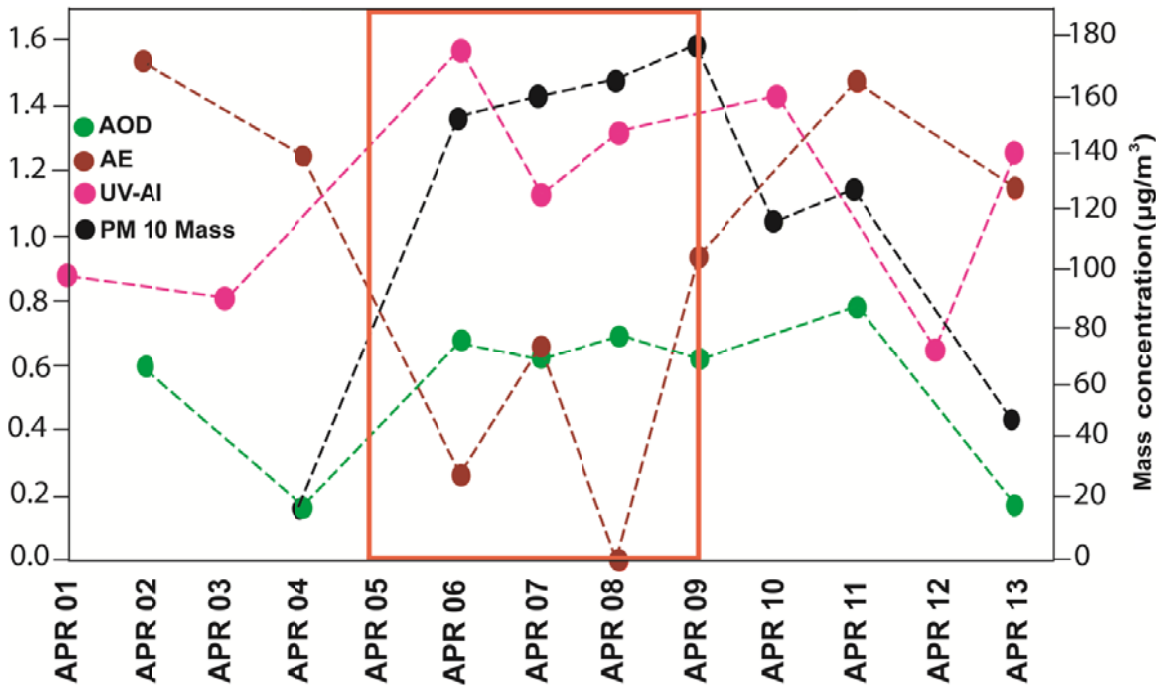


Fig. 3 Variation of daily average of total aerosol mass concentration (in $\mu\text{g m}^{-3}$) calculated from high volume sampler (black filled circle), deep blue aerosol optical depth (AOD) (green filled circle), Angstrom exponent (AE) (brown filled circle) and OMI- Aerosol Index (AI) (pink filled circle) before, during and after the dust storm period. The dates in the range of dotted line represent dusty days.

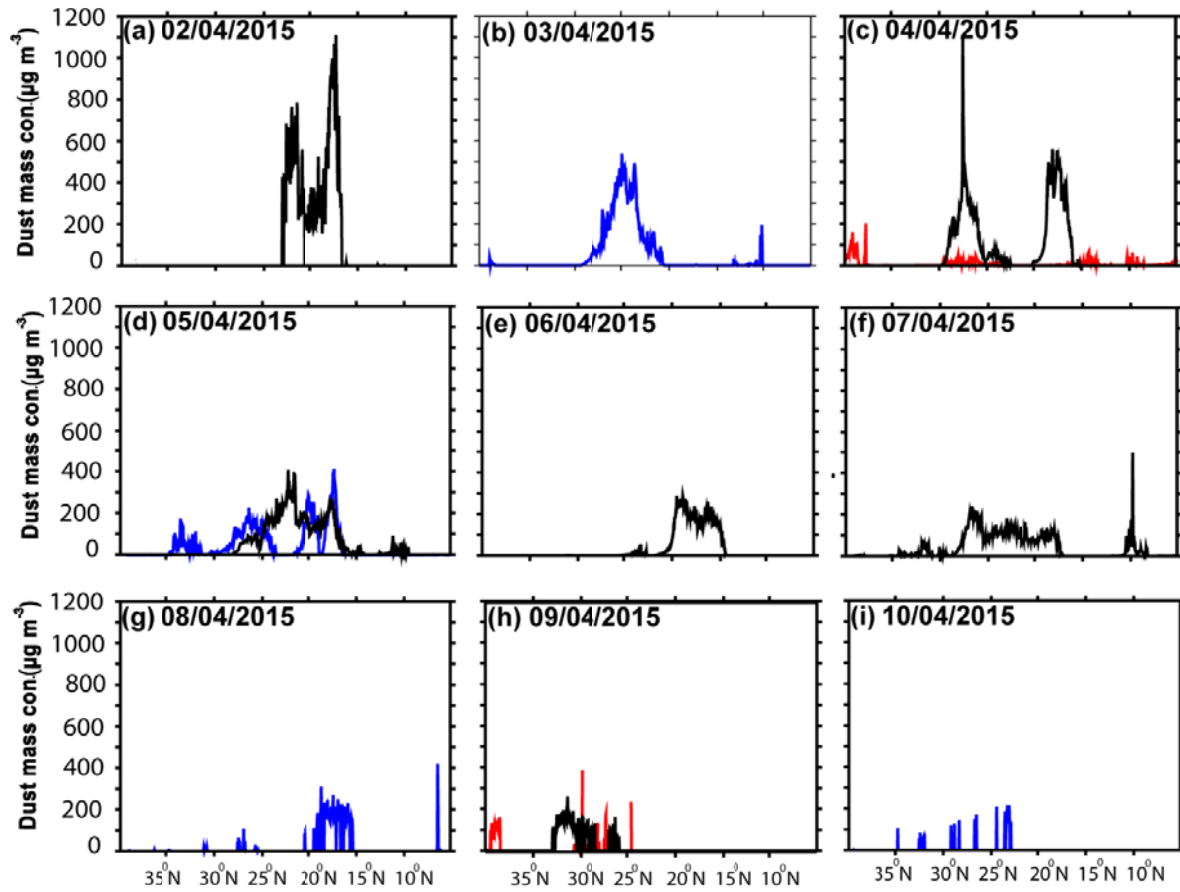


Fig. 4: Daily CALIPSO profile data vertically averaged up to 7 km over different latitude during dust storm period from 02 April- 10 April 2015. Blue represents the CALIPSO profile path over Arabian Sea or center of the ocean (C), Black is profile available near to the source (S) region, and red is profiles available near the receptor (Goa) region (G), during the study period.

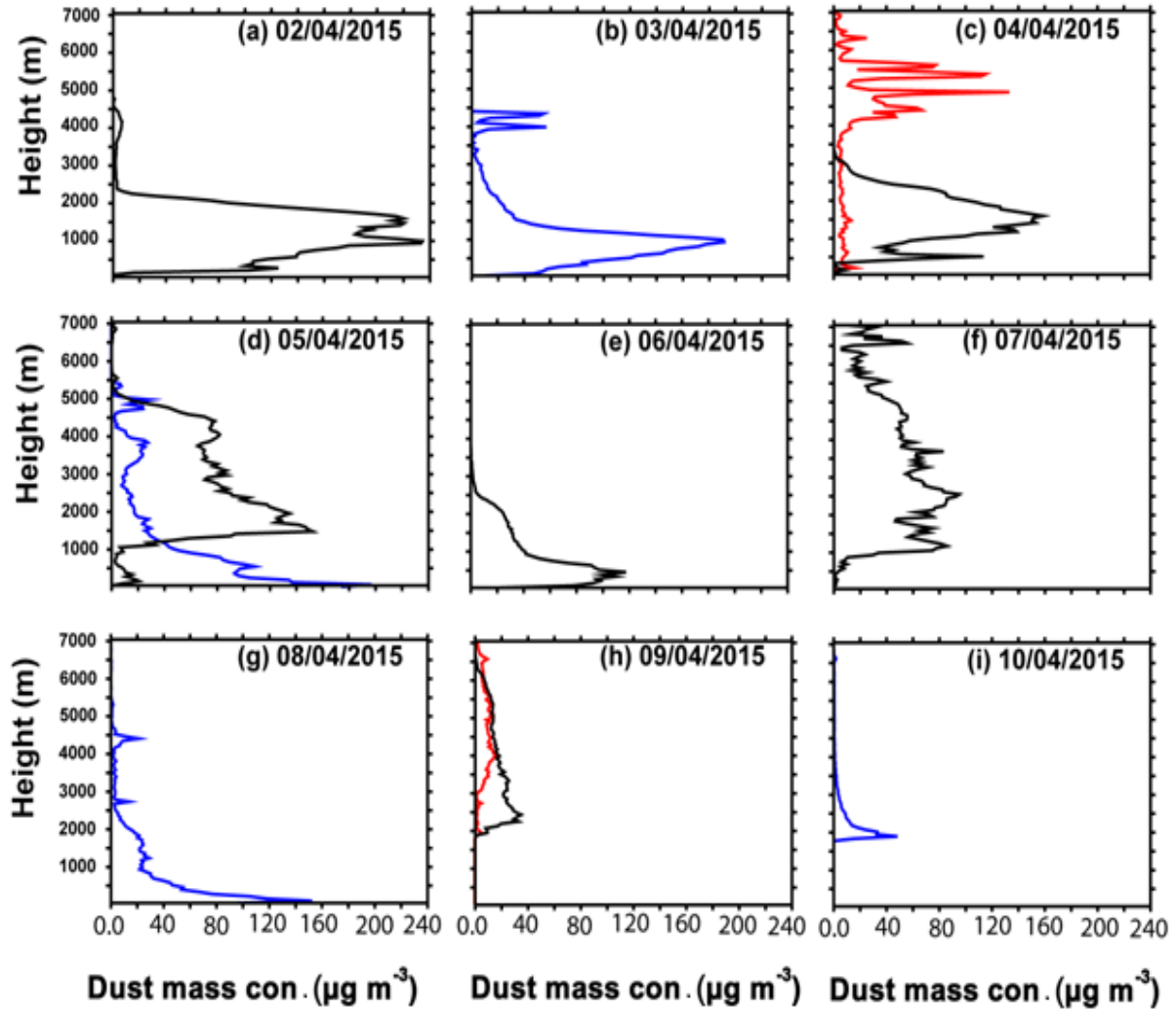


Fig. 5: Latitudinal average of CALIPSO profile from 5o N to 40o N during dust storm period from 02 April- 10 April 2015. Blue represents the CALIPSO profile path over Arabian Sea or center of the ocean (C), Black is profile available near to the source (S) region, and red is profiles available near the receptor (Goa) region (G), during the study period.

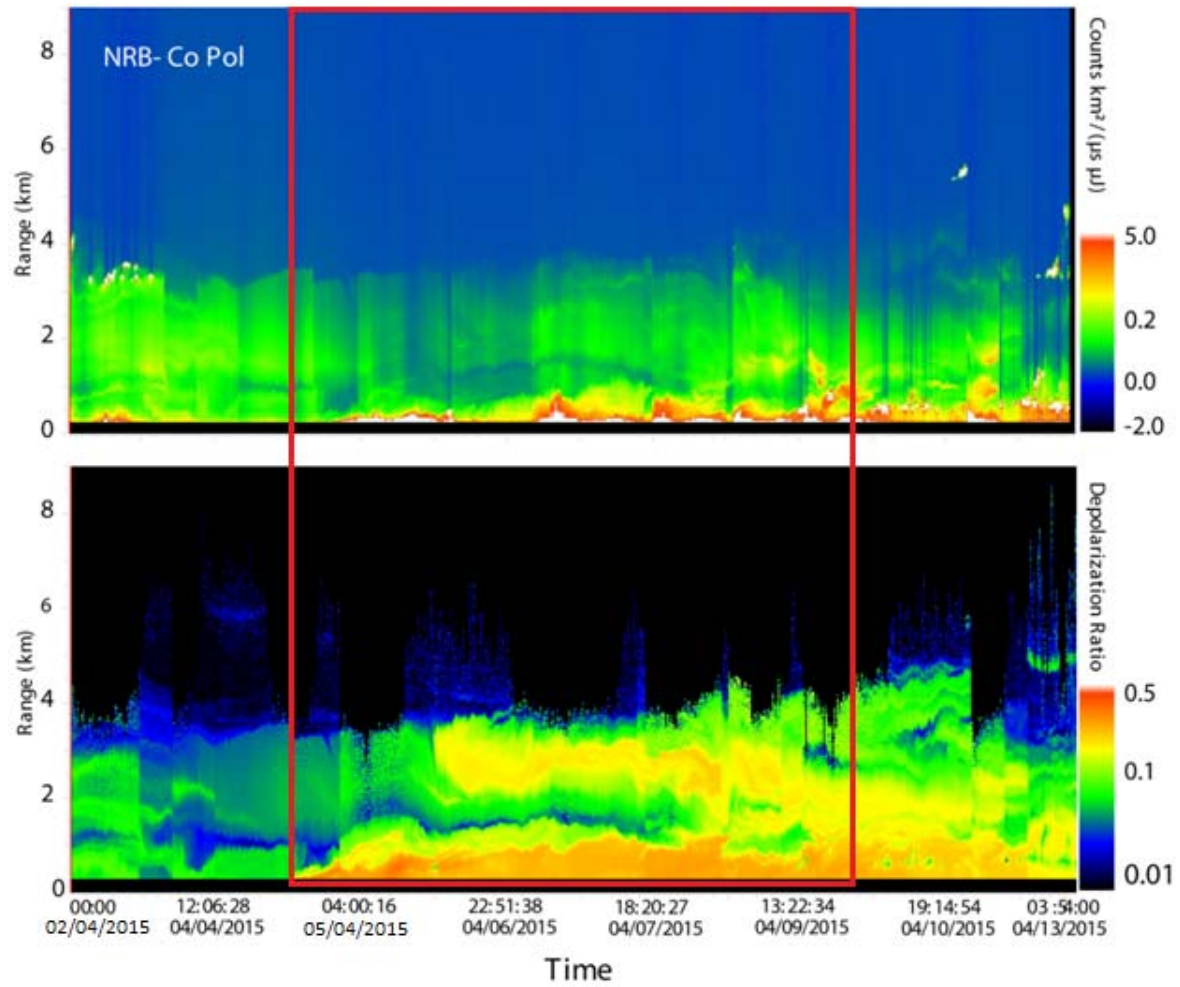


Fig. 6: Height-time cross plot of micro pulse LIDAR profile data during study period. NRB co-pol (above) and Depolarization ratio (below) shows variation in dust layer during study period.

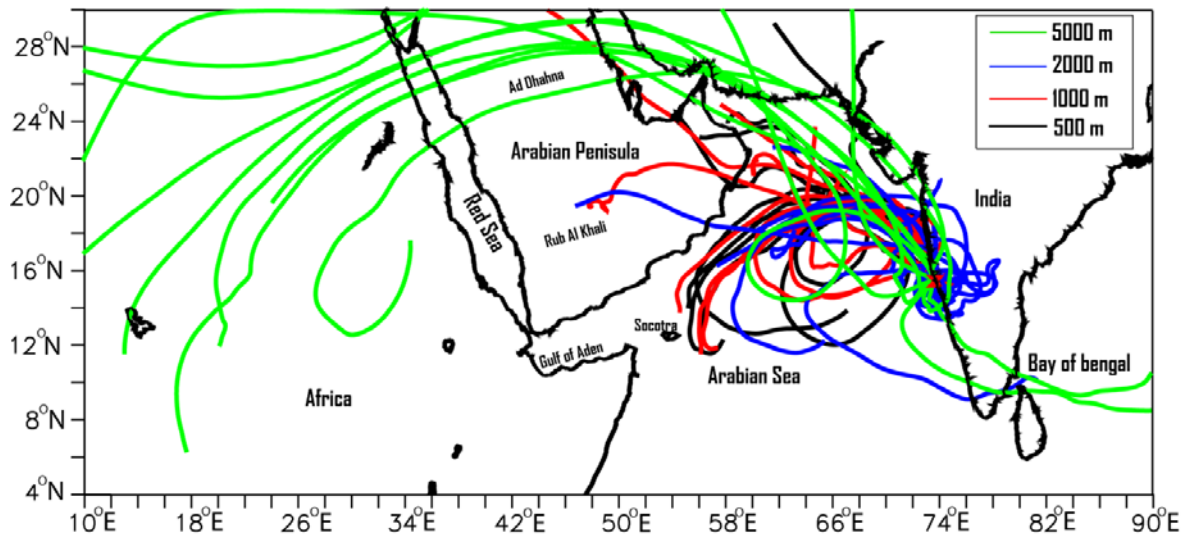


Fig. 7: Seven days back-trajectory of air parcel for 03-13 April, ending at our sampling site at different altitude (5000, 2000, 1000 and 500 m) computed from the HYSPLIT model. Majority of trajectories are passing over the Arabian Peninsula or nearby region of Arabian Peninsula.

Supplementary Material

Quantification of aeolian dust transport towards the Indian peninsular region using satellite and ground-based data- a case study during adust storm over the Arabian Sea.

Aswini M. A.¹, Ashwini Kumar^{1*}, Subrata Kumar Das²

¹CSIR-National Institute of Oceanography, Dona Paula, Goa-403004

²Indian Institute of Tropical Meteorology, Dr. HomiBhabha Road, Pashan, Pune – 411 008

* Corresponding author:

Ashwini Kumar

Geological Oceanography Division

CSIR-National Institute of Oceanography

Dona Paula, Goa-403 004

E-mail: ashwinikumarjha@gmail.com, ashwinik@nio.org

Tel: +91 832 2450368, Fax: +91 832 2450602

Supplementary Figures:

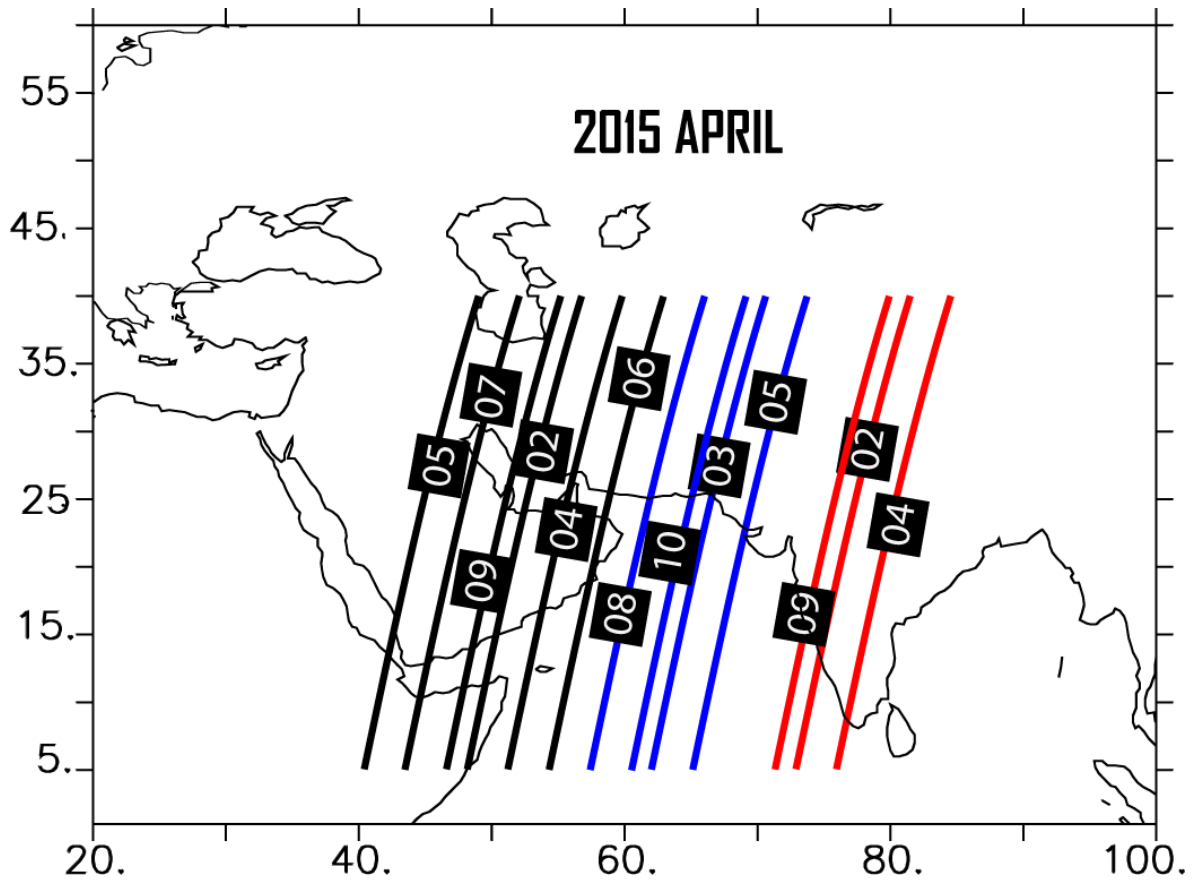


Fig. S1:13 CALIPSO passes over source (black), receptor (red) and Arabian Sea (blue) are shown here with dates in square boxes over the pass during the study period.

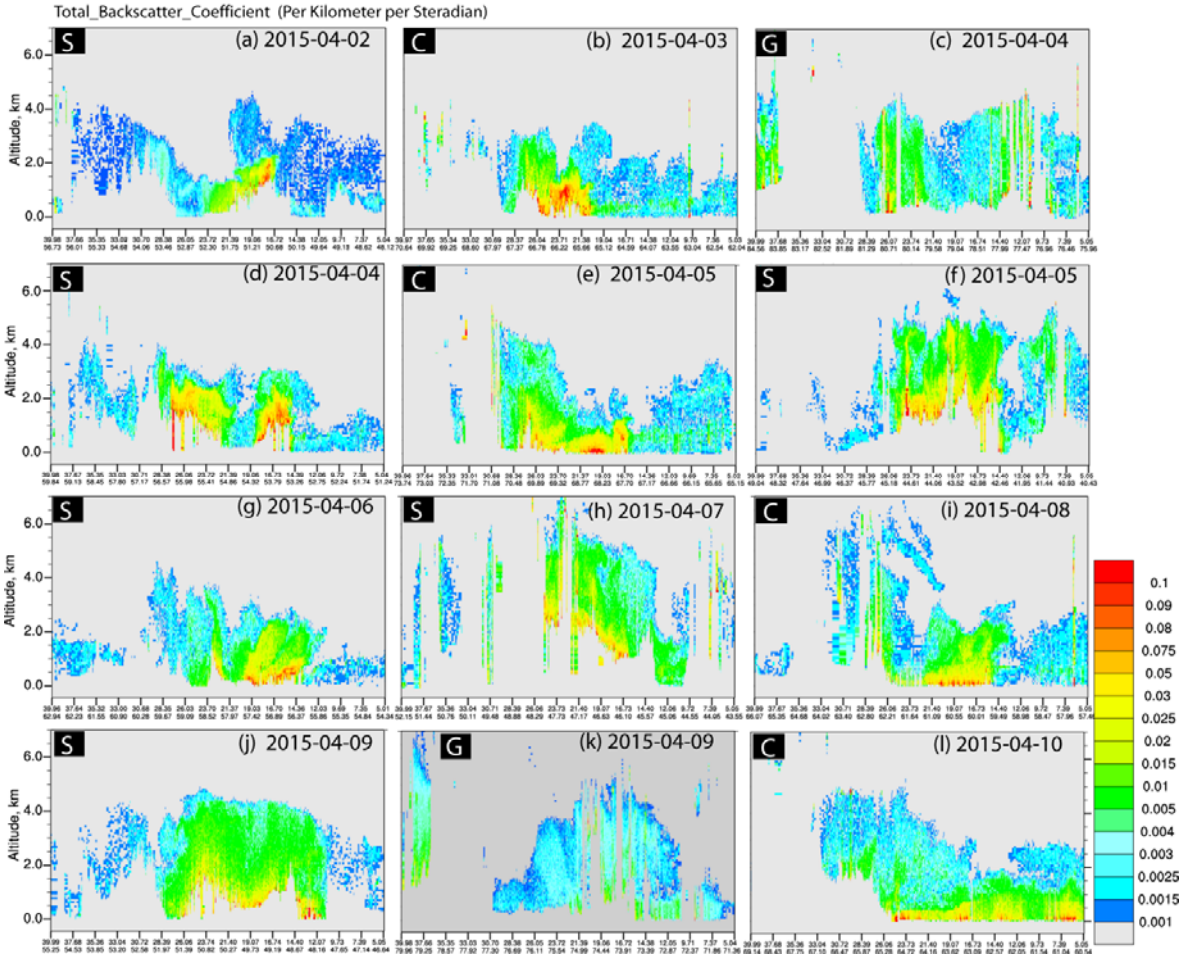


Fig. S2: Total backscatter coefficient (TBC) at 532 nm wavelength from CALIPSO satellite from 02-10 April 2015. S represent profiles available near to the source region, C is profile available over Arabian Sea or center of the ocean and G is profile available near the Goa region.

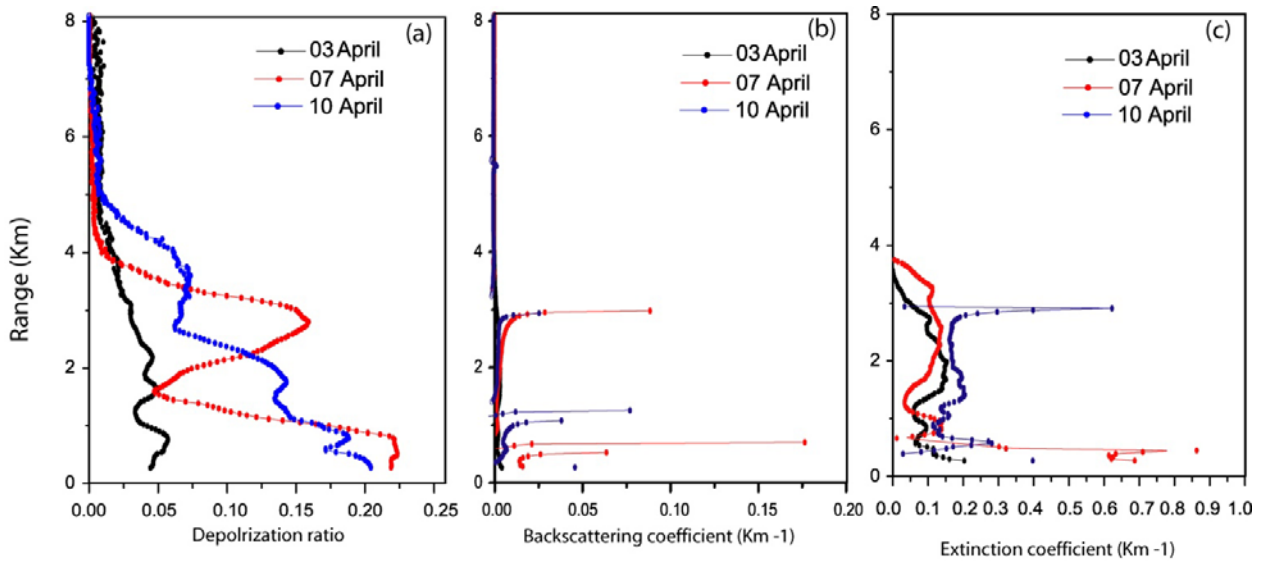


Fig. S3: Daily averaged vertical profiles of LIDAR (a) depolarization ratio, (b) backscatter coefficient and (c) extinction coefficient during the dust storm (07 April), prior (03 April) and after (10 April) dust storm.